Gas Crossover Regulation by Porosity-Controlled Glass Sheet Achieves Pure Hydrogen Production by Buffered Water Electrolysis at Neutral pH

Takahiro Naito,[a] Tatsuya Shinagawa,[a] Takeshi Nishimoto,[a] and Kazuhiro Takanabe*[a]

Near-neutral pH water electrolysis driven by renewable electricity can reduce the costs of clean hydrogen generation, but its low efficiency and gas crossover in industrially relevant conditions remain a challenge. Here, it was shown that electrolyte engineering could suppress the crossover of dissolved gases such as O_2 by regulating their diffusion flux. In addition, a hydrophilized mechanically stable glass sheet was found to block the permeation of gas bubbles, further enhancing the purity of evolved gas from water electrolysis. This sheet had a lower resistance than conventional diaphragms such as Zirfon due to its high porosity and small thickness. A saturated K-phosphate solution at pH 7.2 was used as an electrolyte together with the hydrophilized glass sheet as a gas-separator. This led to a near-neutral pH water electrolysis with 100 mA cm^{-2} at a total cell voltage of 1.56 V with 99.9% purity of produced H_2.

Introduction

Renewable energy is critical for sustainability, but its large scale implementation is hampered by the low energy density and spatiotemporal fluctuations of renewable energy sources. In this context, electrocatalytic processes have worldwide interest because they can convert renewably generated electric power into chemical energy. Using ubiquitous water as a reactant, water electrolysis produces green hydrogen, a core chemical substance in industry. However, the penetration of hydrogen in the current market remains low because it has higher production costs than fossil-fuel-based counterparts.[1] Given that the cost of electricity generated from renewable energy such as solar photovoltaics (PV) and wind has rapidly decreased,[2] a reduction in the system costs is likely critical to the widespread use of green hydrogen in the future.

Nevertheless, further system cost reduction of conventional electrolyzers that are operational at extremely acidic or alkaline pH conditions remains a huge challenge.[3,4] Such pH conditions are critical to maximizing the overall cell efficiency by minimizing the kinetic overpotential and ohmic losses in polymer electrolyte membrane (PEM) or alkaline water electrolyzers.[5] One effort in this direction is to develop an electrolysis cell employing bipolar membrane (BPM) comprising a cation exchange membrane (CEM) and an anion exchange membrane (AEM). The BPM can set acidic and alkaline environments for the hydrogen evolution reaction (HER) and the oxygen evolution reaction (OER), respectively, thus further decreasing the kinetic losses.[6] An efficient BPM requires catalysts that facilitate H_2O dissociation at the interface between the AEM and CEM such as IrO_2[6] for the efficiency improvement. Another effort pressurizes the electrolysis cell whereby the produced gas is already pressurized, and the subsequent compression processes can be skipped.[4,7,8] However, the associated cost reduction is accompanied by a decrease in gas purity; for example, the impurity of H_2 generated by water electrolysis at 100 mA cm^{-2} increased from 0.1% at 1 bar to 0.6% at 20 bar when using Zirfon, a porous diaphragm for the most prevalent water electrolyzer.[9] Furthermore, electrolyzers employing extreme pH conditions suffer from highly corrosive environments, making it necessary to use expensive corrosion-tolerant materials and increasing the system cost. These drawbacks underscore the need for electrolyzers that are operational in milder conditions compatible with the deployment of renewable energy generation on a large scale.

As a non-corrosive reaction medium, near-neutral pH aqueous solution has recently emerged as a next-generation electrolyte. The last decade has witnessed tremendous progress in understanding and improving near-neutral pH water electrolysis. Initially, both half-reactions of the HER and OER were found to suffer from a build-up of local pH gradients under unbuffered near-neutral pH conditions. This leads to an increased concentration overpotential.[10–14] Introducing buffer substances into electrolytes at near-neutral pH thus improved electrocatalytic performance[15,16] plausibly by preventing the local pH shifts.[13,17–19]

[a] T. Naito, Dr. T. Shinagawa, T. Nishimoto, Prof. K. Takanabe
Department of Chemical System Engineering, School of Engineering
The University of Tokyo
7-3-1 Hongo, Bunkyo-ku, Tokyo, 113-8656, (Japan)
E-mail: takanabe@chemsys.t.u-tokyo.ac.jp

ChemSusChem

Research Article
doi.org/10.1002/cssc.202102294

Chemistry Europe
European Chemical
Societies Publishing

Another role of the added substance was suggested in previous studies. A combined experimental and theoretical investigation showed that the electrocatalytic HER rate was largely determined by the mass-transport of the buffer substance functioning as a proton carrier.[17] This finding was corroborated in another study, which reported that enlarging the mass-transport flux of the buffer substance via optimization of electrolyte properties improved electrocatalytic performance. For instance, a highly concentrated aqueous phosphate buffer at near-neutral pH and elevated temperatures was used to minimize the losses associated with mass-transport.[20] In fact, electrocatalytic performance of near-neutral pH in such electrolytes was demonstrated to be comparable to those in an alkaline pH environment using a model Pt cathode and a IrO_x anode at 10 mA cm^{-2}.[20] Efficiently achieving higher reaction rates remains a main challenge of such devices. This calls for further research efforts in this direction.

In addition to the development of electrolyte and electrode for improved performance, industrial deployment of the near-neutral pH water electrolysis requires research efforts in direction of efficient separation of produced gasses compatible with such conditions. Without these separators, the resulting gases can crossover and reach the counter electrode, thus causing back reactions, that is, the oxygen reduction reaction (ORR) or the hydrogen oxidation reaction (HOR). The ORR is a particularly important issue because active catalysts for the HER such as Pt[21–24] and other metals[25–30] also show good ORR performances. Conventional alkaline water electrolyzers use Zirfon as a gas-separator, which consists of ZrO_2 on a polymeric basis.[31] Electrolyzers in a membrane electrode assembly (MEA) configuration employ solid polymer electrolyte (SPE) as a separator. For example, a Nafion membrane made of a perfluorosulfonic acid polymer for PEM water electrolyzer[32] and various types of membranes are made of polyethersulfone polymers with quaternary ammonium groups for AEM water electrolyzers.[33] These separators are the most prevalent for electrolyzers because of their high chemical stability, mechanical strength, thermal stability, and conductivity. However, they cannot simply be employed at near-neutral pH because of the substantially large iR-loss under such conditions. Indeed, the resistance of 0.10 Ω in 7.0 mol kg^{-1} KOH increased by nearly 5-fold in a representative K-phosphate solution (see the Supporting Information, Table S1 for more details) due to the lower conductivity of K-phosphate solutions than the 7.0 mol kg^{-1} KOH.

There have been various strategies reported for gas separation of near-neutral pH water electrolyzers. One pillar of these strategies is a membrane-free configuration.[34–36] The membrane-less electrolyzers rely on the separation of product gases via a flow of electrolytes.[34,36] More specifically, the configuration of flow-by electrodes requires the electrode surfaces to be placed in parallel, and the electrolyte flows between the electrodes. This design prevents transport of generated H_2 and O_2 to the opposite electrodes, thus achieving less gas crossover.[18–20] However, this concept has trade-offs in terms of efficiency, current density, purity of generated gases, and electrode size; for example, a wide gap between electrodes

would increase gas purity but decrease the efficiency.[34] For instance, the cell total voltage reached approximately 2.3 V at a mere current density of 71.5 mA cm^{-2} when achieving > 99% purity of evolved H_2 gas in such a system.[37]

Another strategy employs the concept of electrolyte engineering. In general, the mass-transport flux of dissolved gases is governed by their solubility and diffusion coefficients according to the Fick's law of diffusion.[38] This strategy uses an observation that these properties concurrently decreased with increasing molality of the electrolyte solutions.[5] By employing a concentrated electrolyte (> 1.0 mol kg^{-1}), our previous study demonstrated selective HER in the presence of O_2 at 298 K using a model Pt electrode.[39] Existing theory predicts that, while the diffusion coefficient of generated gases increases at elevating temperatures, the solubility of generated gases decreases.[40,41] This expected trade-off relationship casts a question as to whether this strategy is applicable to the electrolysis system at industrially relevant temperatures of 80 °C or above. In addition, this strategy cannot avoid the crossover of evolved gas bubbles necessitating the use of an additional gas-separator.

Collectively, the industrial deployment of near-neutral pH water electrolysis thus requires the development of a product separation system for both dissolved gases and gas-bubbles while efficiently achieving an industrially relevant reaction rate of 100 mA cm^{-2} or above. Here, we report a near-neutral pH water electrolysis system that employs (1) electrolyte engineering strategy to suppress the crossover of dissolved gases and (2) thin, porous glass-fiber diaphragm that avoids the crossover of produced gas bubbles. Obviously, the glass cannot be utilized for alkaline electrolyzer whose applications are distinctively realized at neutral pH conditions. Quantification of diffusion fluxes of molecules in the rotating disk electrode (RDE) configuration demonstrated the successful regulation of crossover of dissolved gases via electrolyte engineering at increased temperature. The porosity and thickness of the diaphragm was analyzed, suggesting the gas-separation function of the glass sheet with a concurrent lower iR drop. Lastly, near-neutral pH water electrolysis was demonstrated achieving 100 mA cm^{-2} at a total cell voltage of 1.56 V and 100 °C with H_2 purity of 99.9% corresponding to the cell efficiency of 94% with respect to the thermoneutral voltage of 1.47 V.

Results and Discussion

Successful water electrolysis suppresses back reactions, HOR and ORR. These back reactions during water electrolysis can be triggered by supply of the reactant H_2 and O_2 to the anode and cathode, respectively, as either dissolved gas or gas bubbles. This study aims (1) to suppress the crossover of evolved H_2 and O_2 molecules dissolved in the solution by an electrolyte engineering approach and (2) to circumvent the transport of evolved gas bubbles to the counter electrode via a porous glass diaphragm that could not be employed in the corrosive alkaline electrolyzers. Subsequently, a near-neutral pH aqueous water electrolysis was demonstrated at elevated temperatures as well

ChemSusChem

Research Article
doi.org/10.1002/cssc.202102294

**Chemistry
Europe**
European Chemical
Societies Publishing

as industrially relevant current densities for pure H_2 production with comparable efficiency to a conventional water electrolyzer.

Regulation of dissolved gas crossover via electrolyte engineering at elevated temperatures

The concentration gradient of evolved gas molecules drives its crossover during water electrolysis, and Fick's law of diffusion determines its flux [Eq. (1)]:[38]

$$J = -D\frac{C^*}{x} \tag{1}$$

where D is the diffusion coefficient, C^* is the concentration of an evolved gas, and x is the thickness of the diffusion layer. Rigorous quantification of the flux requires the determination of a diffusion-layer thickness. Thus, RDE was adopted in which the mass-transport flux of forced convection is obtained via the following Levich Equation (2):[42]

$$j_{lim} = 0.62n\mathrm{F}\omega^{1/2}\nu^{-1/6}D^{2/3}\Delta C = n\mathrm{F}D\frac{\Delta C}{x} \tag{2}$$

where n defines the number of involved electrons, F is Faraday's constant, ω defines the disk rotation speed, ν is the solution kinematic viscosity, and ΔC represents the difference in the reactant concentrations between the surface and bulk. With these equations, the diffusion layer thickness in the RDE configuration is dictated by Equation (3):

$$\Delta x = 1.62D^{1/3}\nu^{1/6}\omega^{-1/2} \tag{3}$$

By employing the RDE configuration, below the diffusion-limited current density j_{lim}, or Levich current density, was assessed at various temperatures and molalities of electrolyte solutions. Potassium phosphate (K-phosphate) solutions at pH 7.2 (at 25 °C) were adopted as a model electrolyte in which a model Pt cathode and IrO$_x$ anode previously achieved efficiency of water electrolysis comparable to commercialized water electrolyzers though at a low rate of 10 mA cm^{-2}.[20]

Analyzing cyclic voltammograms (CVs) over a polycrystalline Pt disk electrode under Ar, H_2, or O_2 bubbling allowed for experimental determination of diffusion fluxes. Figure S2a shows representative CVs at 25 °C recorded at 0.5, 1.0, and 1.5 mol kg^{-1}, and saturated (2.5 mol kg^{-1}) K-phosphate solutions under those gas atmospheres. A CV consistent with the literature was obtained in a solution of 0.5 mol kg^{-1} K-phosphate with Ar bubbling. Specifically, a cathodic event was observed at around 0.0–0.3 V vs. reversible hydrogen electrode (RHE) due to Pt–H formation followed by its desorption during the anodic scan in the same potential window.[43,44] At potentials more positive than approximately 0.9 V vs. RHE, oxidation currents appeared that originated from Pt–OH or Pt–O formation. These were subsequently reduced during the cathodic scan below 1.2 V vs. RHE.[43,44] The substantial increase in the current density below 0 V vs. RHE was due to the HER. In

a H_2 atmosphere, anodic current densities sharply increased above 0 V vs. RHE, originating from HOR.[10] In the O_2 atmosphere, cathodic current densities were apparent below approximately 0.9 V vs. RHE, and were assigned to the ORR.[25] The redox events were apparent in a saturated electrolyte as shown in the Figure S2 inset although at smaller current densities. Critically, the current densities of both HOR and ORR decreased with increasing molality, consistent with a previous study.[39] Taking current densities at 0.4 V vs. RHE as a representative, the j_{lim} of the ORR was found to be -4.4 mA cm^{-2} in 0.5 mol kg^{-1} K-phosphate solutions, which decreased to -0.08 mA cm^{-2} in saturated K-phosphate solutions. Likewise, the j_{lim} for the HOR was 2.0 and 0.06 mA cm^{-2} in 0.5 mol kg^{-1} and saturated K-phosphate solutions, respectively. The j_{lim} of HOR was smaller than the j_{lim} of ORR because the former requires transfer of 2 electrons while the latter involves a 4-electron transfer.

Theoretically, the diffusion flux follows Equations (1) and (2),[42] which is thus governed by the diffusion coefficient and solubility of gas molecules. In the framework of the Stokes–Einstein model, the diffusion coefficient is determined by the following Equation (4):

$$D = \frac{kT}{3\pi d\mu} \tag{4}$$

The gas solubility was reported to follow the empirical law at 25 °C [Eq. (5)];[40,41]

$$\log\left(\frac{C_{G,0}}{C_G}\right) = \sum(h_i + h_G)C_i \tag{5}$$

in which $C_{G,0}$ is the solubility of gas in pure water, C_G is the solubility of gas in solution, and h is the constant for ion(h_i) and gas(h_G), respectively; C_i is the ion concentration. The latter equation was extended to values below 90 °C [Eq. (6)]:

$$h_G = h_{G,0} + h_T(T - 298.15\ \mathrm{K}) \tag{6}$$

in which $h_{G,0}$ is the h_G value at 25 °C, and h_T is the gas-specific parameter for the compensation of temperature change. Theoretical j_{lim} was computed using these equations (see Table S2 for experimentally determined viscosity, Figure S3 for calculated diffusion coefficient and gas solubility). This was compared with experimentally obtained values. Remarkably, the parity plot in Figure S4 shows that the computational and experimental values agree at 25 °C, thus validating the applicability of these equations for HOR and ORR consistent with the literature.[10] These equations suggest that the diffusion coefficient increases as the temperature increases while the gas solubility decreases. This finding suggests a trade-off relationship between these parameters.

Our experimental investigation was then extended to elevated temperatures. Figure 1a shows CVs recorded in the same gas composition as Figure S2a but at 80 °C as a representative. Similar to the CVs at 25 °C, redox events ascribable to Pt–H formation and desorption as well as Pt
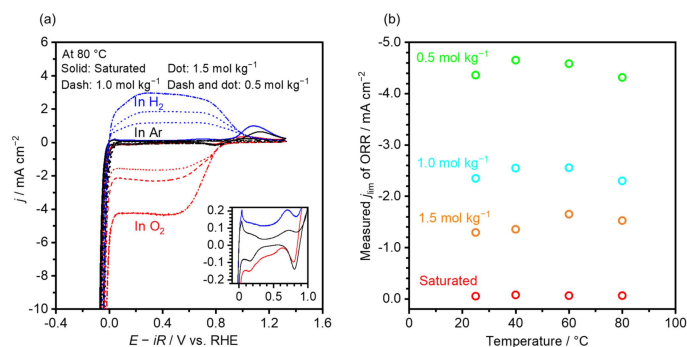
ChemSusChem

Research Article
doi.org/10.1002/cssc.202102294

Chemistry Europe
European Chemical
Societies Publishing

Figure 1. Determination of gas molecule crossover as ORR and HOR (a) Representative CV using a polycrystalline Pt disk electrode under different gas atmospheres (Ar, H_2, or O_2) in 0.5, 1.0, 1.5 mol kg^{-1} or saturated (3.6 mol kg^{-1}) K-phosphate solutions at a scan rate of 50 mV s^{-1} and 3600 rpm at 80 °C. The insets show the magnified views. (b) Measured diffusion-limited current density j_{lim} of ORR at various solution molality of 0.5, 1.0, 1.5 mol kg^{-1}, or saturated as a function of temperature. The j_{lim} values were adopted at 400 mV vs. RHE of the CVs for both the HOR and ORR. pH value of the K-phosphate solutions was adjusted to 7.2 at 25 °C prior to each experiment.

oxidation into Pt—O(H) and its reduction were apparent at 80 °C. The j_{lim} for the ORR and HOR was assessed at 0.4 V vs. RHE. Together with j_{lim} values obtained at different temperatures (see Figure S5 for raw CVs), j_{lim} values of the ORR and HOR are now summarized as a function of temperatures in Figure 1b and Figure S2b, respectively. Figure 1b and Figure S2b show that the $|j_{lim}|$ of both ORR and HOR initially increased below around 40–60 °C with an increase of temperature, which subsequently decreased afterwards regardless of the molalities investigated in the present study. Notably, the experimentally obtained j_{lim} values were found to be substantially smaller than the calculated values above 25 °C for ORR and above 60 °C for HOR (Figure S4) pointing to overestimation of the diffusion coefficient in the conventional model that does not consider the solute-solute interactions.

Critically, the j_{lim} values determined here (Figure 1b and Figure S2b) show that the crossover fluxes of dissolved gas molecules were largely insensitive to the temperature, for example, falling in a range of 0.05–0.08 mA cm^{-2} for ORR and of 0.02–0.07 mA cm^{-2} for HOR in saturated K-phosphate solutions. This quantity is substantially smaller than the industrially targeted reaction rate (e.g., 100 mA cm^{-2} and above). Thus, the regulation of molecule crossover via electrolyte engineering would produce high-purity H_2 via near-neutral pH water electrolysis if the crossover of gas bubbles is circumvented.

Regulation of gas bubble crossover by thin porous sheet

Regulating the transport of gas bubbles requires additional measures including the use of fluid mechanic forces in membrane-less configuration,[34,36] and the use of physical separator[31–33] as detailed in the Introduction. The attainable efficiency at a high rate is limited in the membrane-less configuration,[2] and thus we used a separator in near-neutral pH cells for gas separation. The ideal approach to use the sheet in the near-neutral pH water electrolysis cell would be the zero-gap configuration,[45] in which the anode and cathode sandwich

the separator. This configuration requires the separator to be non-conductive.

The benign near-neutral pH conditions broaden the option of materials for the separator, which are otherwise impossible in conventional electrolysis cells due to their corrosive nature. Among a variety of candidates, silicon-based materials are an ideal candidate with good earth-abundance and cost-efficiency.[46,47] Hence, SiO_2 was selected as the raw material of the separator. It is thermodynamically stable at near-neutral pH regions but easily dissolves under the harsh alkaline pH conditions of conventional alkaline water electrolyzers.[48]

Three representative borosilicate glass-fiber sheets (GS) were purchased from Cytiva: GS-07, GS-12, and GS-16 with varying pore radii of 0.7, 1.2, and 1.6 μm, respectively. Figure 2a shows a photograph and corresponding scanning electron microscopy (SEM) images of GS-16 (see Figure S6 for SEM images of other glass fibers). The glass fiber sheets were woven with glass fibers of several micrometers in diameter (Figure 2a). Table 1 summarizes the properties of these sheets together with a Zirfon diaphragm[49,50] employed in the alkaline electrolyzers (see Table S3 for complete information). GS-16 and GS-12 have the same thickness of 260 μm; GS-07 is thicker by 160 μm. Due to the relatively large pore size and smaller thickness, these GSs all have a porosity as high as approximately 94%. This

Table 1. Properties of gas-separator.[a]

Separator	Pore radius[49,50] [μm]	Thickness[49,50] [μm]	Porosity[49–51] [μm]
GS-16	1.6	260	93.6
GS-12	1.2	260	93.6
GS-07	0.7	420	94.4
Zirfon	0.1	500 ± 50	55 ± 10

[a] Values of pore size and thickness were obtained from manufacturing companies.[49,50] The porosity for the Zirfon was also obtained from the company,[49] and that for the glass fiber sheets was calculated using the density of the fiber and weight per unit area of the product.[50,51] See Table S3 for complete information including costs.
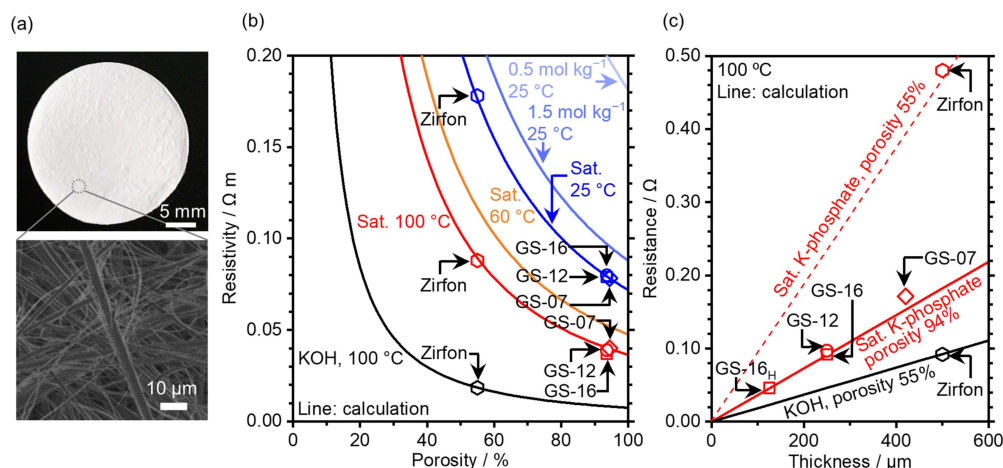
ChemSusChem

Research Article
doi.org/10.1002/cssc.202102294

**Chemistry
Europe**
European Chemical
Societies Publishing

Figure 2. Resistivity and resistance of gas-separators in representative electrolyte solutions. (a) Photograph and SEM image of GS-16. (b) Resistivity in 0.5, 1.5, or 2.5 (saturated) $mol\,kg^{-1}$ K-phosphate solutions or 7.0 $mol\,kg^{-1}$ KOH solutions at 25, 60, or 100 °C. (c) Resistance of glass fiber sheets (GS-16, GS-12, and GS-07) and Zirfon at 100 °C in 4.1 $mol\,kg^{-1}$ (saturated) K-phosphate solutions or 7.0 $mol\,kg^{-1}$ KOH solutions. The open symbols denote the values measured by impedance spectroscopy (see Figure S1 for the cell configuration), and lines represent the calculated values. The pH value of the K-phosphate solutions was adjusted to 7.2 at 25 °C prior to each experiment. The GS-16$_H$ with a thickness of 130 µm in the panel (c) was obtained by splitting GS-16 into two pieces (see Experimental Section for details), and the obtained sheet was subjected to hydrophilization treatment (see the text) and thus labeled with subscript H.

feature contrasts themselves from Zirfon that has a pore radius of 0.1 µm and a porosity of around 55%.

The non-conductive nature of these sheets increases the resistivity, and thus their structure needs to be optimized for lessened iR loss and in turn higher cell efficiency. The resistance, R, is a function of resistivity and cell constant from a fundamental viewpoint [Eq. (7)]:

$$R = \rho K_{cell} \tag{7}$$

The resistivity of a porous medium consisting of spheres is expressed by the following empirical Equation (8):[52–54]

$$\rho = \rho_0 \frac{1}{\varepsilon^{1.5}}, \tag{8}$$

in which ρ is the resistivity of the porous medium, ρ_0 is the resistivity of the electrolyte, and ε is the porosity of the medium. The cell constant is determined by the following Equation (9):[55]

$$K_{cell} = \frac{l}{A}, \tag{9}$$

where l and A are the specific length and cross-sectional area of the electrochemical cell, respectively.[55] Taken together, the resistance is anticipated to be lower for a thinner sheet with larger porosity at a given geometric area.

With this theoretical background in mind, a subsequent study experimentally assessed the resistivity and the sheet thickness. Figure 2b plots the resistivity as a function of porosity. The resistivities of K-phosphate solutions decreased with increasing molality and temperatures consistent with a previous report (see Table S4 for the measured values of

resistivity for the K-phosphate solutions).[20] At 25 °C, the resistivity of K-phosphate at 0.5 $mol\,kg^{-1}$ was 0.18 $\Omega\,m$, which decreased to 0.07 $\Omega\,m$ at 2.5 $mol\,kg^{-1}$ (saturated) and further to 0.04 $\Omega\,m$ at 4.1 $mol\,kg^{-1}$ (saturated) at 100 °C. With gas-separators, the resistivity was determined to be approximately 0.04 and 0.09 $\Omega\,m$ for the GS sheets and Zirfon in saturated (4.1 $mol\,kg^{-1}$) K-phosphate, respectively. A slight variation of the resistivity among GSs might originate from the distinct tortuosity of sheets[56] (see Figure S6 for the morphology of sheets). These values agreed nicely with the calculations from Equation (8), thus validating the model for GSs.

Equation (8) also indicates that the resistivity would decrease with a more conductive electrolyte. A supporting electrolyte was thus added to the 4.1 $mol\,kg^{-1}$ K-phosphate solutions, which decreased the resistivity by 25% in the case of K_2SO_4 (see Figure S7 for optimization of the ratio of saturated K-phosphate to K_2SO_4) as indicated in Figure S8a. Nevertheless, these quantities were still inferior to that at 7.0 $mol\,kg^{-1}$ KOH at 100 °C. This picture was, however, changed when the film thickness was considered. Thinner sheets could be fabricated due to the mechanical strength of GSs. Figure 2c and Figure S8b compile resistance as a function of the sheet thickness at 100 °C. The resistance value of 0.16 Ω for GS at 420 µm was decreased to 0.09 Ω at 260 µm and then to 0.05 Ω at 130 µm. Strikingly, this value of 0.05 Ω was superior to the 0.09 Ω obtained in the industrially relevant 7.0 $mol\,kg^{-1}$ KOH solution with Zirfon. These quantitative analyses demonstrated that the near-neutral pH water electrolysis with GS achieved as small iR losses as the conventional alkaline water electrolyzers.

The gas-separation capability of GSs was then examined. From a fundamental viewpoint, the permeability of gas-separator is related to a bubble point pressure expressed in the following Laplace Equation (10):[57]

$$\Delta P = \frac{2\gamma \cos\theta}{r} \quad (10)$$

in which ΔP is the pressure difference applied across the gas-separator, γ is the surface tension at the liquid-air interface, θ is the contact angle of the liquid with the gas-separator material, and r is the pore radius in sheets. A larger value of the ΔP indicates a higher value of threshold pressure for bubble nucleation, thus leading to less permeability of the bubbles. The contact angle and the pore radius are variables that determine ΔP because the surface tension at the liquid-air interface does not vary with the identity of the separator. More specifically, smaller pore sizes and smaller contact angle are beneficial in decreasing the permeability. Given that the pore size, or the porosity, is a decisive parameter of resistance as described in Figure 2, GS-16 was herein subjected to hydrophilization treatment by soaking the GS in piranha solutions to decrease the contact angle (the hydrophilized, half-thickness GS-16 is herein denoted as GS-16$_H$). Although the porous nature of the GS did not allow for experimental determination of their contact angles, the literature reported that hydrophilized SiO$_2$ achieved contact angles as low as 2°.[58] Figure S9 summarizes the impact of hydrophilization treatment on the bubble retention. The series resistance using the pristine GS-16 was 0.7 Ω that was found to become 2.2 Ω after the chronopotentiometry (CP) testing of water electorlysis at 100 mA cm^{-2} (see below), most likely due to the pore-blocking by the evolved gases. When hydrophilized, however, the GS-16 (denoted as GS-16$_T$) experienced almost negligible increase in the resistance after the CP. The obtained resistance value of 0.8 Ω after the CP was greatly smaller than the value obtained with Zirfon in K-phosphte solution (1.3 Ω). More tellingly, by hydrophlization

treatment, GS-16 experienced lessened series resistance value by 1.4 Ω during water electrolysis, corresponding to a decrease of iR loss as much as 140 mV at 100 mA cm^{-2}.

Experimental assessment of the gas purity directly addressed the gas-separation function of the sheet. The cell configuration shown in Figure 3a was developed for this purpose in which the anode and cathode chambers were separated by an electrode-separator assembly to collect evolved gas separately in each chamber. The purity of gas in this study was defined as the concentration of gas of interest over the sum of H$_2$ and O$_2$ concentration at the cell gas outlet. The purity at a current density of 100 mA cm^{-2} using GS-16$_H$ is summarized in Figure 3b. Strikingly, the purities of evolved H$_2$ and O$_2$ were as high as ca. 99.9 and 99.3%, respectively. This purity is comparable with the values of > 99.5% reported with KOH solution and Zirfon.[59,60] The difference in purities between H$_2$ and O$_2$ may originate from their distinct mass-transport fluxes (see Section S4 of the Supporting Information for extended discussion). Overall, these results show that the GS sheets in the saturated K-phosphate solutions can simultaneously achieve low resistance and high gas purity comparable to the existing alkaline water electrolyzers.

Demonstration of water electrolysis using glass fiber sheets in saturated K-phosphate solutions at near-neutral pH

The previous sections disclosed that the saturated phosphate solution was demonstrated to suppress the crossover of dissolved gaseous molecules at the elevated temperatures, and the GS-16$_H$ was found to be capable of blocking the crossover of gas bubbles while concurrently achieving small iR losses. After combining these components with a model Pt/Pt mesh
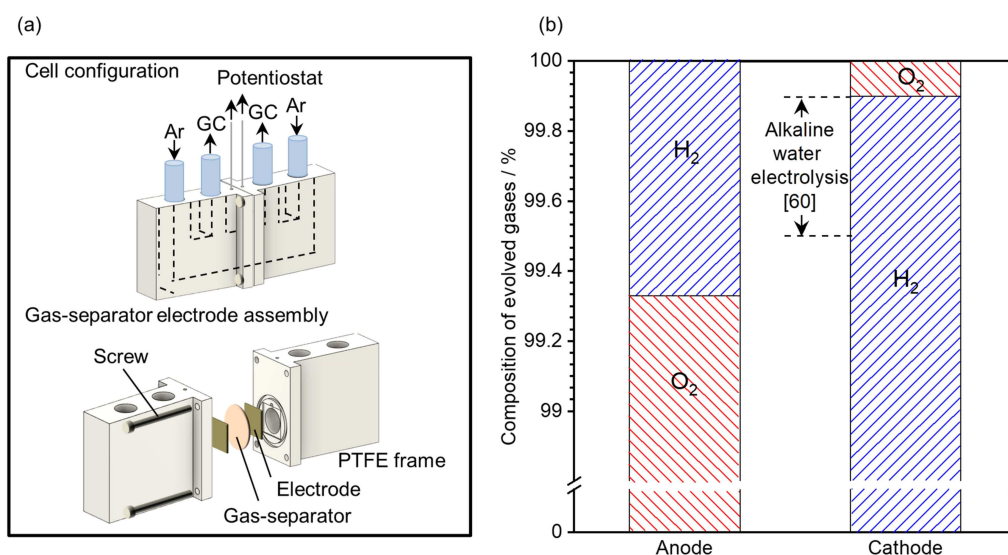
(a)

(b)

Figure 3. Experimental determination of evolved gas purity. (a) Cell configuration developed to measure the purity of evolved gas. The effective surface area of the electrodes was 0.79 cm^2 (a circle of 1 cm diameter). (b) Measured purity of gases evolved at an anode and cathode chambers, with flowing Ar at 0.5 ml min^{-1}. The purity was measured using the IrO$_x$/Ti felt anode, the Pt/Pt mesh cathode, and the GS-16$_H$ in the saturated K-phosphate solution at 100 °C. pH value of the K-phosphate solutions was adjusted to 7.2 at 25 °C prior to each experiment.

cathode and IrO$_x$/Ti felt anode, this section next examines the near-neutral pH water electrolysis performance. Anode- and cathode-sandwiched gas-separators were used as the zero-gap configuration,[45] which was fixed by polytetrafluoroethylene (PTFE) frame and screws (see Figure S10 for the cell illustration).

Figure 4 shows the breakdown of total cell voltage for near-neutral pH and alkaline water electrolysis at an applied constant current density of 100 mA cm^{-2} at 100 °C (see Figures S11 and S12 for raw data). The alkaline condition employed 7.0 mol kg^{-1} KOH as an electrolyte, and NiFeO$_x$/Ni foam as an anode instead of the IrO$_x$ catalyst because NiFeO$_x$ is known to be a highly active OER catalyst under alkaline conditions, and IrO$_x$ degrades during OER under alkaline conditions.[20] Notably, the high alkalinity of 7.0 mol kg^{-1} KOH solution did not facilitate the determination of a half-reaction performance, and the total overpotential of both HER and OER is displayed in this figure. The total cell voltage was 1.83 V at 0.5 mol kg^{-1} at 25 °C with K-phosphate electrolyte solutions, which decreased by 70 mV at 2.5 mol kg^{-1} (saturated). The improvement most likely arose from the acceleration of mass transport as we previously reported.[20] Nevertheless, even when using the concentrated solution, the total cell voltage is still inferior to alkaline conditions by 110 mV. The difference in *iR* loss value between Figures 4 and 2c plausibly originated from generated bubbles during electrolysis[61] and wiring.[62]

Elevation of the reaction temperature was considered to be beneficial in improving kinetics and mass transport during water electrolysis. Herein the water electrolysis performance was assessed at 100 °C, and the voltage breakdown is detailed in Figure 4. Strikingly, a current density of 100 mA cm^{-2} was reached at a total cell voltage as small as 1.56 V in the saturated K-phosphate solutions of 4.1 mol kg^{-1} at 100 °C. This value corresponded to the cell efficiency of 94 and 75 % with respect to the thermoneutral voltage of 1.47 V and reversible voltage of 1.17 V.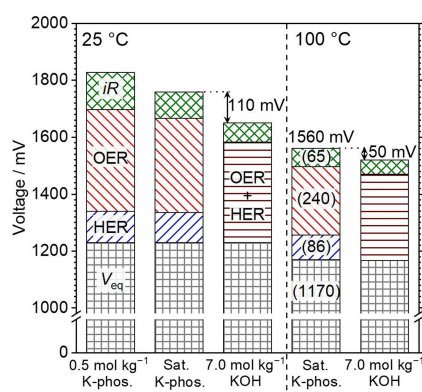 The concurrently measured faradaic efficiency (FE) for both H$_2$ and O$_2$ was almost 100 % continuously for 1 h (Figure S13), which is consistent with the near unity purity of gases discussed in Figure 3b. In contrast, the alkaline system in 7.0 mol kg^{-1} KOH solutions required 1.51 V to reach 100 mA cm^{-2}, consistent with industrially related values.[4] Quantitatively, therefore, the near-neutral pH water electrolysis achieved a comparable performance to the alkaline electrolyzers with a difference of merely 50 mV at 100 mA cm^{-2}. Among this 50 mV, around 15 mV was accounted for by the difference in series resistance (i.e., 0.65 and 0.50 Ω for the K-phosphate and KOH solutions, respectively). The remaining 35 mV is reasoned to originate from the kinetic overpotentials.

The longevity of the cell is another figure of merit in assessing the system performance. Figure 5a shows the CP at 100 mA cm^{-2} for 24 h indicating that the initial overall cell voltage of 1.56 V increased by merely 5 mV after 24 h. X-ray photoelectron spectroscopy (XPS) analysis in Figure S14 showed no apparent change of surface chemical state. Subsequent on-off testing in Figure 5b suggested that the system would retain its integrity upon start-up and shut-down cycles. SEM micrographs of GS-16$_H$ before and after the 24 h CP testing in Figure S6 disclosed that its diameter remained to be 3.5 μm, demonstrating the high tolerance of GSs. Figure S15 plots the cell voltage in 7.0 mol kg^{-1} KOH solution with NiFeO$_x$/Ni foam anode and Pt/Pt mesh cathode for comparison (see Figure S16 for the data obtained with 1.0 mol kg^{-1} KOH electrolyte solutions). This alkaline system required 1.51 V to reach 100 mA cm^{-2} consistent with industrial values;[4] this increased to a value of 1.53 V after 24 h.

Our study was extended to higher current densities at 400 mA cm^{-2}, and the resulting voltage breakdown is shown in Figure S17. The total cell voltage was anticipated to reach 1.91 V with almost equal contribution from the OER, HER, and the *iR* loss in saturated K-phosphate solutions using GS-16$_H$ at 100 °C: This assessment was experimentally validated by the full-cell testing at 400 mA cm^{-2} in Figure S18. This analysis points to the need for concurrent efforts on these three aspects when reaching higher rates. For instance, development of active OER and HER catalysts seems essential in enhancing the performance, but the engineering surface morphology to facilitate gas-bubble removal from catalyst surfaces is a key issue[54] and is also likely dependent on the properties of the electrolyte.[63,64] Another direction includes the development of more conductive electrolyte. Simply adding supporting electrolyte increased conductivity of the solution as discussed in Figure S8, which however was accompanied by a loss in cell performance (see Figure S18), suggesting kinetic losses due to the poisoning of the catalyst surface by the adsorption of sulfate ions.[65] These aspects call for integrated research efforts toward the entire system rather than a single component.

Figure 4. Voltage breakdown of water electrolysis at 100 mA cm^{-2} at 25 °C and 100 °C in various electrolyte solutions of 0.5, 2.5 (saturated at 25 °C), 4.1 (saturated at 100 °C) mol kg^{-1} phosphate with GS-16$_H$ or 7.0 mol kg^{-1} KOH solutions with Zirfon. V_{eq} denotes the reversible voltage. "HER" and "OER" were the overpotentials for HER and OER, respectively. These overpotentials were determined by electrocatalytic testing in buffered solutions in every solution under Ar bubbling. The *iR* loss was determined with a measured impedance value.

Conclusions

This study investigated efficient near-neutral pH water electrolysis for pure H$_2$ production at reaction rates compatible with industrial applications. Low solubility and low diffusion coef-
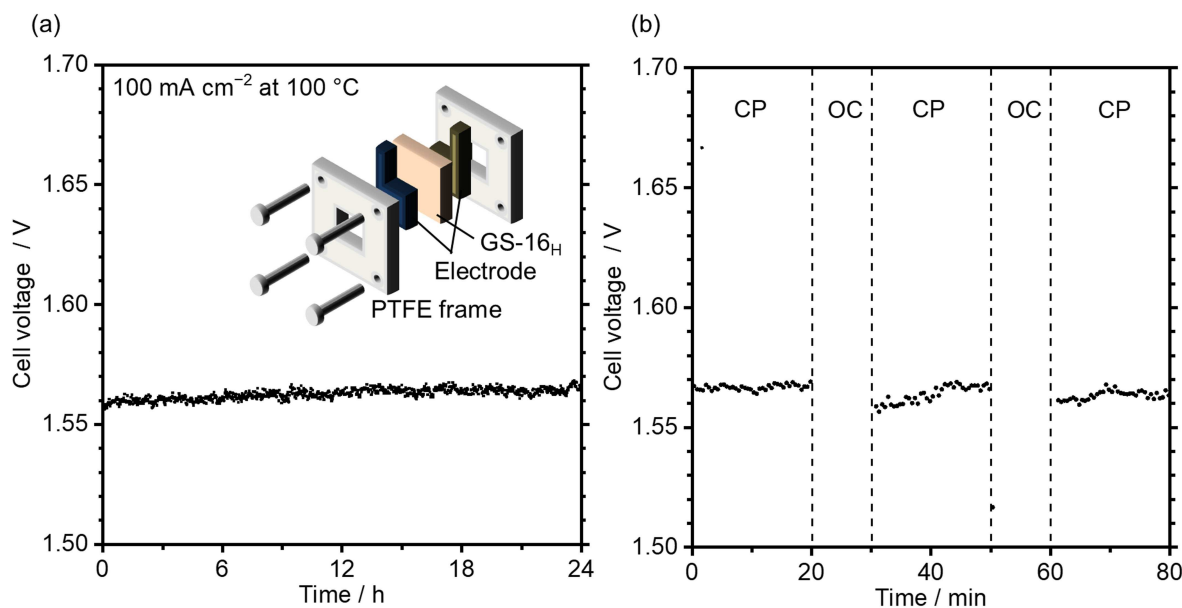
Figure 5. Demonstration of near-neutral pH water electrolysis. (a) Prolonged CP testing at 100 mA cm^{-2} using an IrO$_x$/Ti felt anode and a Pt/Pt mesh cathode in 4.1 mol kg^{-1} (saturated) K-phosphate with GS-16$_H$. The inset illustration is a cell configuration used in the demonstration. (b) On–off cycling of water electrolysis in densely buffered solutions at 100 °C. On–off testing results were obtained by periodic CP at 100 mA cm^{-2} for 20 min with an interval of 10 min at open-circuit (OC) condition using a Pt/Pt mesh cathode and an IrO$_x$/Ti felt anode in saturated K-phosphate with GS-16$_H$. The measurement was performed after CP for 24 h as shown in (a). pH level of K-phosphate solutions was adjusted to 7.2 at 25 °C prior to the measurements.

ficients of dissolved H$_2$ and O$_2$ gases in concentrated phosphate buffer solutions almost eliminated the diffusion-limited current densities of the H$_2$ oxidation and O$_2$ reduction reactions, which can be interpreted as minimized crossover of the dissolved gases during water electrolysis. These diffusion-limited currents were largely insensitive to temperature. The gas-bubble crossover at buffered neutral pH was successfully regulated via glass-made sheets (i.e., GS) as a gas separator, which are not usable in alkaline electrolyzers because they dissolve. Assessment of the porosity and thickness of the sheets showed that the GSs together with saturated K-phosphate solutions can achieve a small iR-loss comparable to or less than Zirfon with 7.0 mol kg^{-1} KOH solutions. The iR loss values originating from the GSs were reduced by 140 mV during water electrolysis at 100 mA cm^{-2} by a hydrophilization treatment to the GSs. Experimental testing with an electrolysis cell employing the GS-16$_H$ exhibited approximately 99.9% purity of evolved H$_2$, thus demonstrating the feasibility of GSs as the gas separator. Current densities of 100 mA cm^{-2} were achieved at as low total cell voltage as 1.56 V with negligible performance losses after 24 h of operation corresponding to 94% of cell efficiency with respect to the thermoneutral voltage of 1.47 V (this experiment used saturated K-phosphate solution as electrolyte at 100 °C with GS-16$_H$ as the gas-separator in the catalytic testing). This performance is comparable to the established alkaline counterpart. At larger current densities, however, voltage breakdown analysis showed that hydrogen and oxygen evolution reaction kinetic loss and iR loss all contribute substantially to imperfection, thus calling for concurrent research efforts to both electrodes and electrolytes in future studies. Overall, our findings demonstrate that near-neutral pH water electrolysis is an alternative to existing acidic and alkaline water electrolysis, thus paving the way for penetration of green H$_2$.

Experimental Section

Chemicals: The following chemicals were used: H$_2$Cl$_6$Pt$_6\cdot$H$_2$O (99.9%, FUJIFILM Wako Pure Chemical Corporation), KOH (ACS reagent, Sigma–Aldrich), H$_3$PO$_4$ (ACS reagent, Sigma–Aldrich), HClO$_4$ (assay 70%, Sigma–Aldrich), Na$_3$IrCl$_6\cdot x$H$_2$O, H$_2$C$_2$O$_4$ ($\geq$99%, Sigma–Aldrich), Na$_2$CO$_3\cdot$H$_2$O ($\geq$9.5%, Sigma–Aldrich), H$_2$SO$_4$(ACS reagent, Sigma–Aldrich), H$_2$O$_2$ (for atomic absorption spectrochemical analysis, FUJIFILM Wako Pure Chemical Corporation), HCl (ACS reagent, Sigma–Aldrich), HNO$_3$ (SAJ first grade, Sigma–Aldrich), KCl (99.999%, Sigma–Aldrich), Ni(NO$_3$)$_2\cdot$6H$_2$O (97.0%, FUJIFILM Wako Pure Chemical Corporation), Fe(NO$_3$)$_3\cdot$9H$_2$O (99.0%, FUJIFILM Wako Pure Chemical Corporation), urea (ACS reagent, Sigma-Aldrich), as well as GS/A, GS/C, and GS/F (denoted as GS-16, GS-12, GS-07, respectively) microfiber glass sheets (Cytiva), Zirfon pearl UTP 500 (Agfa).

Electrolyte preparations: K-phosphate solutions were employed as an electrolyte. Concentrated KOH solutions were mixed into concentrated H$_3$PO$_4$ aqueous solution to obtain targeted concentration of K-phosphate solutions at pH 7.2. The molality in our study represents that of phosphate ions (the sum of H$_2$PO$_4^-$ and HPO$_4^{2-}$). The detailed protocol is the same as that described in our previous study.[20]

Determination of gas-separator electrolyte properties: The resistivity of electrolyte solution was assessed by potentiostatic electrochemical impedance spectroscopy (PEIS) using a 16-channel research-grade potentiostat system (VMP3, BioLogic Science Instruments). The measurement was performed in a two-electrode

ChemSusChem

Research Article
doi.org/10.1002/cssc.202102294

Chemistry
Europe
European Chemical
Societies Publishing

system with two Pt wires separated by 2.0 cm using an electrochemical cell with cell constant K_{cell} of 0.6 cm^{-1} that was determined using 1.0 mol kg^{-1} KCl solution as a reference. The viscosity of K-phosphate solutions was measured with a viscometer (SVM3001, Anton Paar) at varying concentrations and temperatures. The resistance of the gas-separators was determined by measuring the resistance of electrode assembly with and without gas-separators, using a cell configuration illustrated in Figure S1 (see Figure S1 for detailed description of the measurement).

Hydrophilization of glass sheets: Hydrophilization of glass sheet was conducted by immersing sheets in piranha solutions for 30 min.[58] The piranha solutions were prepared by mixing 12 mL of 75% H_2SO_4 solution and 4 mL 30% H_2O_2 solution. After immersion, the sheets were cleaned with ultrapure water several times and then dried in air. The series resistances before and after this hydrophilization on GS-16 are shown in Figure S9.

Preparation of thinner glass sheets: GS-16 glass sheets were mechanically split in halves. The resistivity of split sheets was measured using the cell configuration shown in Figure S1 to confirm the same resistivities of both sheets and thereby the same thickness of the filters.

Electrode preparation: The IrO_x electrodes were fabricated by electrochemical deposition following a reported protocol[66] on a titanium felt substrate. The pH level of the deposition bath containing 0.4 mM of $Na_3IrCl_6 \cdot xH_2O$ and 2 mM of $H_2C_2O_4$ was adjusted to 10 by adding $Na_2CO_3 \cdot H_2O$ and held at 35 °C for four days prior to the deposition. A Ti felt (ST/Ti/20/150/67 m NIKKO TECHNO) with a geometric size of 1×1 cm^2 was immersed in 35% HCl aqueous solutions for 30 min to remove surface oxides. This was then washed by ultrapure water several times and immediately used. The electrochemical deposition was conducted using a three-electrode configuration with Pt mesh (Nilaco) and Hg/Hg_2Cl_2 (saturated with KCl) as the counter and reference electrodes, respectively. IrO_x was deposited onto the felt as a working electrode by immersing the felt in the prepared deposition bath and applying a constant current density of 140 µA cm^{-2} for 70 ks. CV using each fabricated electrode was recorded in 0.1 mol kg^{-1} $HClO_4$ to ensure identical properties.

A platinized platinum (Pt/Pt mesh) electrode was fabricated by electrochemical deposition following a reported recipe[67,68] with a Pt mesh (Nilaco) as the substrate. Prior to electrochemical deposition, the Pt mesh was immersed in aqua regia for 1 min. (The aqua regia was prepared by mixing HCl and HNO_3 at a volume ratio of 3:1). The mesh was then washed with copious amount of ultrapure water. Subsequently, the electrochemical deposition was conducted using a three-electrode configuration with Pt mesh (Nilaco) and Hg/Hg_2Cl_2 (saturated with KCl) as the counter and reference electrodes, respectively. Platinum was deposited onto the platinum mesh as a working electrode by immersing the mesh in a deposition bath and applying a constant potential of −0.1 V vs. Hg/Hg_2Cl_2 for 15 min. CV used each fabricated electrode and was recorded at 0.1 mol kg^{-1} $HClO_4$ to ensure identical properties.

A $NiFeO_x$ electrode was next prepared by the hydrothermal synthesis following the literature.[69] Prior to the synthesis, the Ni foam was washed by immersing the foam in 0.1 mol kg^{-1} HCl, ultrapure water and ethanol sequentially for 5 min each. The Ni foam was then transferred to a 100-mL Teflon-lined stainless-steel autoclave together with 80 mL of solution containing 1 mmol of $Ni(NO_3)_2 \cdot 6H_2O$, 1 mmol of $Fe(NO_3)_3 \cdot 9H_2O$, and 5 mmol of urea. These were heat-treated at 120 °C for 12 h. The autoclave was then naturally cooled to room temperature.

Electrochemical determination of dissolved gas diffusion fluxes: A diffusion-limited current density j_{lim} was experimentally deter-

mined using a RDE configuration in three electrode system. Prior to testing, a polycrystalline Pt disk with a 3.0 mm diameter (BAS, Inc) was first polished with a 1-µm diamond and then with 0.05 µm alumina (both purchased from BAS, Inc.). The surface was further electrochemically treated by CV in 1.0 mol L^{-1} $HClO_4$. A Hg/Hg_2Cl_2 (saturated with KCl) and a Pt wire were used as the reference and counter electrodes, respectively. Before and during all measurements, Ar (99.9999%), H_2 (99.9999%), or O_2 (99.9995%) gas was continuously supplied to the cell. CV was conducted at disk-rotation speeds of 3600 rpm and at a scan rate of 1 mV s^{-1}. The current-potential relationship described in this study was iR-corrected using a resistance value determined by the PEIS at 1 kHz with 10 mV amplitude. The cell was equipped with a jacket (Water-Jacketed glass cell; BAS Inc.), and its temperature was controlled by an external equipment (NCB-1210, Eyela). All current densities are expressed in terms of the geometric electrode surface area. The j_{lim} of the ORR was determined by taking the difference of current densities between in O_2 and Ar atmospheres at 0.4 V vs. RHE. Likewise, the j_{lim} of the HOR was determined by comparing the CVs in H_2 and Ar atmosphere.

Determination of gas purity at the cell outlet: Purity of evolved gases via water electrolysis was determined by measuring the gas composition at the cell outlet. Electrolysis was conducted in two-electrode systems, and the home-made PTFE cell is shown in Figure 3a. The cell separates the anodic and cathodic chambers with gas-separators sandwiched in between. Both chambers were filled with around 4 mL of electrolyte solutions. The fabricated IrO_x/Ti felt and Pt/Pt mesh with the geometric surface area of 10 mm × 10 mm were used as the anode and cathode, respectively. A glass sheet was placed between the chambers with a geometric surface area of 0.79 cm^2 in a circular shape with a diameter of 1 cm. Ar (99.9999%) was used as a carrier gas, which was supplied to the cell headspace at a flow rate of 0.5 mL min^{-1}. The composition of gas outlet was determined using on-line gas chromatography (GC; Shimadzu Cooperation, GC-2014) with Shincarbon-ST column (SHINWA CHEMICAL INDUSTRIES LTD.) equipped with thermal conductivity detector (TCD). The system temperature was controlled by using silicone rubber heating belt. All current densities are expressed in terms of the geometric electrode surface area.

Half-cell electrocatalytic testing: Electrocatalytic measurements for the half-cell reactions, namely the HER and the OER, were conducted in a three-electrode system. The Pt/Pt mesh or fabricated IrO_x/Ti felt with the geometric surface area of 10 mm × 10 mm were used as the working electrode for the HER or OER testing, respectively, with a Hg/Hg_2Cl_2 (saturated with KCl) reference electrode and a Pt wire counter electrode. Before and during all measurements, H_2 (99.9999%) or O_2 (99.9995%) gas was continuously supplied to the cell for the HER or OER testing. The CV was performed at 1 mV s^{-1}. The current-potential relationship described in this study was iR-corrected using a resistance value determined by the PEIS at 1 kHz with 10 mV amplitude. The employed cell is shown in Figure S10, and its temperature was controlled by placing the cell in an oil bath. All current densities are expressed in terms of the geometric electrode surface area.

Electrolysis testing: Water electrolysis testing was conducted in a zero-gap configuration as illustrated in Figure S10. The configuration employed the IrO_x/Ti felt anode (10×10 mm^2) and Pt/Pt mesh cathode (10×10 mm^2) sandwiching the gas separator (12×12 mm^2). These were fixed using a PTFE frame and screw. The electrode-separator assembly was placed in a glass cell, and its temperature was controlled by an oil bath. CP was performed, and the outlet gas composition was determined by GC-TCD using Ar (99.9999%) carrier gas at a flow rate of 100 mL min^{-1}. All current densities were expressed in terms of the geometric electrode surface area.

Characterizations. Surface chemical states of the IrO_x/Ti felt anode and the Pt/Pt mesh cathode were characterized by XPS (JPS-9010MC, JEOL) using Mg K_α radiation as shown in Figure S14. The binding energy scale was calibrated using the C 1s peak at 285.0 eV. The morphologies of the glass fiber sheets were characterized by SEM (JSM-IT800, JEOL) as shown in Figure S6.

Acknowledgements

Conflict of Interest

The authors declare no conflict of interest.

Data Availability Statement

The data that support the findings of this study are available from the corresponding author upon reasonable request.

[1] S. E. Hosseini, M. A. Wahid, *Renewable Sustainable Energy Rev.* **2016**, *57*, 850–866.
[2] D. V. Esposito, *Joule* **2017**, *1*, 651–658.
[3] Ø. Ulleberg, *Int. J. Hydrogen Energy* **2003**, *28*, 21–33.
[4] A. Buttler, H. Spliethoff, *Renewable Sustainable Energy Rev.* **2018**, *82*, 2440–2454.
[5] M. F. Lagadec, A. Grimaud, *Nat. Mater.* **2020**, *19*, 1140–1150.
[6] B. Mayerhöfer, D. McLaughlin, T. Böhm, M. Hegelheimer, D. Seeberger, S. Thiele, *ACS Appl. Energ. Mater.* **2020**, *3*, 9635–9644.
[7] A. Ursúa, L. M. Gandía, P. Sanchis, *Proc. IEEE* **2011**, *99*, 1–17.
[8] G. Chisholm, L. Cronin, *Storing Energy* Elsevier, Amsterdam, **2016**, pp. 315–343.
[9] P. Trinke, P. Haug, J. Brauns, B. Bensmann, R. Hanke-Rauschenbach, T. Turek, *J. Electrochem. Soc.* **2018**, *165*, F502–F513.
[10] D. Strmcnik, M. Uchimura, C. Wang, R. Subbaraman, N. Danilovic, D. van der Vliet, A. P. Paulikas, V. R. Stamenkovic, N. M. Markovic, *Nat. Chem.* **2013**, *5*, 300–306.
[11] T. Shinagawa, A. T. Garcia-Esparza, K. Takanabe, *ChemElectroChem* **2014**, *1*, 1497–1507.
[12] T. Takashima, K. Ishikawa, H. Irie, *ACS Catal.* **2019**, *9*, 9212–9215.
[13] I. Katsounaros, J. C. Meier, S. O. Klemm, A. A. Topalov, P. U. Biedermann, M. Auinger, K. J. J. Mayrhofer, *Electrochem. Commun.* **2011**, *13*, 634–637.
[14] M. Auinger, I. Katsounaros, J. C. Meier, S. O. Klemm, P. U. Biedermann, A. A. Topalov, M. Rohwerder, K. J. J. Mayrhofer, *Phys. Chem. Chem. Phys.* **2011**, *13*, 16384–16394.
[15] W. Sheng, Z. Zhuang, M. Gao, J. Zheng, G. Chen, Y. Yan, *Nat. Commun.* **2015**, *6*, 5848.
[16] T. Shinagawa, M. T.-K. Ng, K. Takanabe, *ChemSusChem* **2017**, *10*, 4155–4162.
[17] T. Shinagawa, K. Takanabe, *J. Phys. Chem. C* **2015**, *119*, 20453–20458.
[18] L. D. S. Muñoz, A. Bergel, D. Féron, R. Basséguy, *Int. J. Hydrogen Energy* **2010**, *35*, 8561–8568.
[19] T. Shinagawa, K. Takanabe, *ChemSusChem* **2017**, *10*, 1318–1336.
[20] T. Naito, T. Shinagawa, T. Nishimoto, K. Takanabe, *ChemSusChem* **2020**, *13*, 5921–5933.
[21] N. M. Marković, H. A. Gasteiger, P. N. Ross Jr., *J. Phys. Chem.* **1995**, *99*, 3411–3415.
[22] M. D. Maciá, J. M. Campiña, E. Herrero, J. M. Feliu, *J. Electroanal. Chem.* **2004**, *564*, 141–150.
[23] E. Fabbri, S. Taylor, A. Rabis, P. Levecque, O. Conrad, R. Kötz, T. J. Schmidt, *ChemCatChem* **2014**, *6*, 1410–1418.
[24] T. Shinagawa, K. Takanabe, *J. Power Sources* **2015**, *287*, 465–471.
[25] S. Guo, D. Li, H. Zhu, S. Zhang, N. M. Markovic, V. R. Stamenkovic, S. Sun, *Angew. Chem. Int. Ed.* **2013**, *52*, 3465–3468; *Angew. Chem.* **2013**, *125*, 3549–3552.
[26] N. M. Marković, T. J. Schmidt, V. Stamenković, P. N. Ross, *Fuel Cells* **2001**, *1*, 105–116.
[27] B. Han, C. E. Carlton, J. Suntivich, Z. Xu, Y. Shao-Horn, *J. Phys. Chem. C* **2015**, *119*, 3971–3978.
[28] V. R. Stamenkovic, B. Fowler, B. S. Mun, G. Wang, P. N. Ross, C. A. Lucas, N. M. Markovic, *Science* **2007**, *315*, 493–497.
[29] V. Stamenkovic, B. S. Mun, K. J. J. Mayrhofer, P. N. Ross, N. M. Marković, J. Rossmeisl, J. Greeley, J. K. Nørskov, *Angew. Chem. Int. Ed.* **2006**, *45*, 2897–2901; *Angew. Chem.* **2006**, *118*, 2963–2967.
[30] X. Huang, Z. Zhao, L. Cao, Y. Chen, E. Zhu, Z. Lin, M. Li, A. Yan, A. Zettl, Y. M. Wang, X. Duan, T. Mueller, Y. Huang, *Science* **2015**, *348*, 1230–1234.
[31] J. Brauns, J. Schönebeck, M. R. Kraglund, D. Aili, J. Hnát, J. Žitka, W. Mues, J. O. Jensen, K. Bouzek, T. Turek, *J. Electrochem. Soc.* **2021**, *168*, 014510.
[32] H. Ito, T. Maeda, A. Nakano, H. Takenaka, *Int. J. Hydrogen Energy* **2011**, *36*, 10527–10540.
[33] S. Miyanishi, T. Yamaguchi, *Phys. Chem. Chem. Phys.* **2016**, *18*, 12009–12023.
[34] X. Pang, J. T. Davis, A. D. Harvey, D. V. Esposito, *Energy Environ. Sci.* **2020**, *13*, 3663–3678.
[35] S. M. H. Hashemi, P. Karnakov, P. Hadikhani, E. Chinello, S. Litvinov, C. Moser, P. Koumoutsakos, D. Psaltis, *Energy Environ. Sci.* **2019**, *12*, 1592–1604.
[36] J. C. Bui, J. T. Davis, D. V. Esposito, *Sustain. Energy Fuels* **2020**, *4*, 213–225.
[37] S. Mohammad, H. Hashemi, M. A. Modestino, D. Psaltis, *Energy Environ. Sci.* **2015**, *8*, 2003–2009.
[38] P. Atkins, J. D. Paula, *Atkins' Physical Chemistry, eighth ed.*, W. H. Freeman and Company, New York, **2006**.
[39] T. Shinagawa, K. Takanabe, *J. Phys. Chem. C* **2016**, *120*, 1785–1794.
[40] C. Hermann, I. Dewes, A. Schumpe, *Chem. Eng. Sci.* **1995**, *50*, 1673–1675.
[41] S. Weisenberger, A. Schumpe, *AIChE J.* **1996**, *42*, 298–300.
[42] A. J. Bard, L. R. Faulkner, *Electrochemical Methods: Fundamentals and Applications*, Wiley, New York, **2010**.
[43] P. Daubinger, J. Kieninger, T. Unmüssig, G. A. Urban, *Phys. Chem. Chem. Phys.* **2014**, *16*, 8392–8399.
[44] A. Berná, V. Climent, J. M. Feliu, *Electrochem. Commun.* **2007**, *9*, 2789–2794.
[45] R. Phillips, C. W. Dunnill, *RSC Adv.* **2016**, *6*, 100643–100651.
[46] U. S. Department of the Interior, *MINERAL COMMODITY SUMMARIES 2020*, **2020**.
[47] U. S. Department of the Interior, *Rare Earth Elements – Critical Resources for High Technology*, **2002**.
[48] F. K. Crundwell, *ACS Omega* **2017**, *2*, 1116–1127.
[49] Cytiva, available online: https://www.cytivalifesciences.com/en/us/shop/whatman-laboratory-filtration/glass-and-quartz-microfiber-filter/binder-less-glass-microfiber-filter (accessed on 20 May 2021).
[50] Technical Data Sheet ZIRFON PERL UTP 500 Separator membrane for alkaline electrolysis, AGF-16, **2020**.
[51] L. Chen, S. Ding, Z. Liang, L. Zhou, H. Zhang, C. Zhang, *Aerosol Sci. Technol.* **2017**, *51*, 1082–1092.
[52] M. J. Martínez, S. Shimpalee, J. W. Van Zee, *J. Electrochem. Soc.* **2009**, *156*, B80–B85.
[53] B. Tjaden, S. J. Cooper, D. J. Brett, D. Kramer, P. R. Shearing, *Curr. Opin. Chem. Eng.* **2016**, *12*, 44–51.
[54] M. T. de Groot, A. W. Vreman, *Electrochim. Acta* **2021**, *369*, 137684.
[55] R. Bataller, J. M. Gandia, E. Garcia-Breijo, M. Alcañiz, J. Soto, *Electrochim. Acta* **2015**, *82*, 263–272.
[56] F. Yang, M. J. Kim, M. Brown, B. J. Wiley, *Adv. Energy Mater.* **2020**, *10*, 2001174.

[57] PH. Vermeiren, R. Leysen, H. Beckers, J. P. Moreels, A. Claes, *J. Porous Mater.* **2008**, *15*, 259–264.

[58] T. Son, E. Yang, E. Yu, K. H. Oh, M.-W. Moon, H.-Y. Kim, *J. Mech. Sci. Technol.* **2017**, *31*, 5407–5414.

[59] D. Pletcher, F. C. Walsh, *Industrial electrochemistry. 2nd ed.*, Blackie Academic & Professional, London, **1990**.

[60] P. Haug, M. Koj, T. Turek, *Int. J. Hydrogen Energy* **2017**, *42*, 9406–9418.

[61] A. Roy, S. Watson, D. Infield, *Int. J. Hydrogen Energy* **2006**, *31*, 1964–1979.

[62] M. I. Gillespie, F. van der Merwe, R. J. Kriek, *J. Power Sources* **2015**, *293*, 228–235.

[63] W. Xu, Z. Lu, X. Sun, L. Jiang, X. Duan, *Acc. Chem. Res.* **2018**, *51*, 1590–1598.

[64] X. Zhao, H. Ren, L. Luo, *Langmuir* **2019**, *35*, 5392–5408.

[65] E. Protopopoff, P. Marcus, *J. Electrochem. Soc.* **1988**, *135*, 3073–3075.

[66] M. A. Petit, V. Plichon, *J. Electroanal. Chem.* **1998**, *444*, 247–252.

[67] A. M. Feltham, M. Spiro, *Chem. Rev.* **1971**, *71*, 177–193.

[68] I. Lee, K–Y Chan, D. L. Phillips, *Appl. Surf. Sci.* **1998**, *136*, 321–330.

[69] Z. Lu, W. Xu, W. Zhu, Q. Yang, X. Lei, J. Liu, Y. Li, X. Sun, X. Duan, *Chem. Commun.* **2014**, *50*, 6479–6482.